Advances in Reliability, Safety and Security, Part 9 – Kołowrocki, Dąbrowska (eds.)
 ISBN 978-83-68136-21-0 (printed), ISBN 978-83-68136-08-1 (electronic)

Advances in Reliability, Safety and Security

ESREL 2024
Monograph Book Series

Condition Monitoring Of Wind Turbine Blade Bearings

Wenxian Yang[a], Zian Wu[b], Yunyu Ma[b], Kexiang Wei[b], Andrew Ball[a], Robert Cattley[a]

[a]*School of Computing and Engineering, University of Huddersfield, Huddersfield HD1 3DH, United Kingdom*
[b]*School of Mechanical Engineering, Hunan Institute of Engineering, Xiangtan 411104, China*

Abstract

The pitch bearing of a wind turbine plays a crucial role in achieving precise blade positioning and ensuring the safety and power generation efficiency of the turbine. Since the faults developed in such bearings are often associated with long downtime and high maintenance costs, it is of significance to detect their faults as early as possible. However, due to the non-integer cycle rotation of the pitch bearing during normal operation, traditional vibration analysis methods are incapable of detecting the faults in such bearings. To address this issue, an innovative pitch bearing monitoring technique is proposed in this paper by leveraging the advantages of thermal imaging analysis and deep learning. In this study, outer race faults were emulated on a specially designed pitch bearing test rig. Then, temperature distributions across the bearing structure were captured using a thermal imaging camera. Subsequently, the captured images are used to train the YOLOv5 algorithm to detect faults. Finally, the proposed technique is validated by comparing its fault detection results with stress measurements that are more reliable, but not feasible to use in practice. It has been demonstrated that the proposed thermal imaging-based technique is capable of accurately detecting pitch bearing faults, even when the bearing is not in rotation.

Keywords: wind turbine, pitch bearing, condition monitoring, thermography

1. Introduction

In light of pressing global issues, such as climate change and environmental pollution, there is an ongoing shift in global energy consumption toward cleaner sources, gradually replacing fossil fuels. Wind energy stands out as a key player in the clean energy sector, and its global installations continue to experience rapid growth. The Global Wind Energy Council (GWEC) forecasts that by 2024, annual onshore wind power installations will surpass the 100 GW milestone, while offshore wind power installations are projected to exceed 25 GW by 2025. Looking ahead to 2027, the world is expected to have a total wind power installation capacity of 680 GW, with 130 GW being installed offshore (GWEC, 2023). Today, many countries are making substantial strides in wind power development. For example, it anticipates that by 2050, domestic wind power installations in China will reach an impressive 2,400 GW, constituting a substantial 33.8% of the total installed capacity in the country (National Development and Reform Commission, 2015). Wind power is also vital in helping the UK achieve its net-zero emissions targets. The UK now possess around 12.7 GW of connected offshore wind energy across 44 wind farms totaling over 2,500 turbines, but the UK government has set an ambitious target to deliver 50 GW offshore wind installed capacity by 2050. To cater to the demands of this rapidly expanding market, modern wind turbine designs have evolved to be exceptionally advanced to achieve lighter weight, larger power generation capacity, and higher efficiency designs. Yet, this progress also results in a more intricate and compact configuration for the turbine's structures, and consequently elevates the likelihood of turbine failures (Hofmann, 2014).

The long-term wind power practice has demonstrated that pitch bearings are one of the most fragile components among all wind turbine components (Wilkinson et al., 2010; Bi et al., 2014; Liu et al., 2019). The failure of pitch bearings can result in the loss of blade control and even damage to the entire turbine system. Due to the high cost of maintenance and replacement of pitch bearings, their condition monitoring and fault diagnosis are crucial for reducing operational and maintenance costs and improving system reliability. In recent years,

research on the condition monitoring and early fault detection of blade pitch bearings has gained increasing attention. Currently, common methods for pitch bearing condition monitoring include vibration analysis (Liu et al., 2019; Zvokelj et al., 2010), finite element method (FEM) (Plaza et al., 2015), oil analysis (Liu, 2007; Bai et al., 2011), acoustic emission (AE) (Van Hecke et al., 2016), etc. For example, Liu et al. (2020) proposed an empirical wavelet thresholding method to remove heavy noise, extract weak fault signals, and successfully achieved fault diagnosis of pitch bearings. Pan Y. et al. (2019) introduced a systematic approach based on cyclic domain resampling to map time-series signals into the angular domain, eliminating the time attribute and reducing the number of circular domain signals using segment-wise aggregated approximation with neighbourhood correlation, and successfully detected frequency variations in vibration signals when initial faults occurred. Vásquez et al. (2019) provided a model-based solution to detect pitch bearing damage, where blade angle residual between healthy and monitored local models was used to raise anomalies. However, the method was only demonstrated in FAST simulation with artificially seeded bearing faults, and there were not any hardware tests for validation. He et al. (2019) and Pan D. et al. (2019) introduced a methodology for monitoring the condition of blade pitch by analysing electric current signals obtained from the electric pitch actuator. This approach has undergone validation in MW-scale commercial wind turbines with naturally damaged pitch bearings. It is noteworthy that the efficacy of this technology was demonstrated in scenarios where only one pitch bearing exhibited defects. However, the detection results may be influenced by variations in pitch operating conditions. Likewise, Kandukuri et al. (2019) similarly aimed to leverage electric current signals acquired from the electric pitch actuator for pitch bearing fault detection, employing support vector machine (SVM) as a discerning tool. Sandoval et al. (2020) proposed a novel approach for low-speed bearing fault diagnosis based on permutation and spectral entropy measurements, and successfully differentiated different fault types based on different entropy values. Compared to vibration-based condition monitoring and fault diagnosis methods, acoustic emission-based methods have advantages such as strong resistance to noise interference, higher sensitivity, and wider frequency response. After subsequent signal processing, the acoustic emission frequency signal becomes clearer and purer, allowing for fault identification and determination, particularly in the processing of low-frequency signals. Liu and Wang et al. (2020) proposed a discrete/random separation-based cepstrum editing (DRS-CEL) method to extract weak fault features from the original acoustic emission signal, edit the cepstrum using discrete/random separation, further filter residual noise leaked by DRS-CEL using morphological envelope analysis, and demodulate the denoised signal, thereby inferring specific bearing fault types in the frequency domain. Wei et al. (2020) proposed a new Normal Behaviour Modelling (NBM) method to predict wind turbine electric pitch system failures using supervisory control and data acquisition (SCADA) information. In the data preprocessing stage of the proposed method, the operational state codes from turbine programmable logic controller are applied to filter SCADA data to remove interferential information and improve data quality. Zhang and Márquez et al. (2022) proposed a new algorithm called Time Convolution Enhanced Bayesian Search (TCABS) to search for the 'synthetic period' of unknown signals. After estimating the window length, they used the Split Bayesian Augmented Lagrangian (SBAL) algorithm based on the split window technique to construct a time-varying model and determined the type of pitch bearing fault using envelope analysis. Zhang and Liu et al. (2022) also introduced a method called Bayesian and Adaptive Kalman Augmented Lagrangian (BAKAL) to filter signals under time-varying conditions. This method employed a two-step search (i.e., coarse search and fine search) to handle the filtering process based on the Bayesian Augmented Lagrangian (BAL) framework. Furthermore, linear effects, nonlinear effects, and their sparsity were considered when constructing the model. Finally, superior fault diagnosis performance was achieved by handling the ambiguity in the spectrum through signal resampling in the order domain. Chen et al. (2023) integrated Bladed and MATLAB using Python and a cloud platform for integrated life cycle simulation to reduce simulation time. They proposed a three-dimensional modelling approach to calculate crack propagation in pitch bearings throughout their entire life cycle and accurately identified and predicted the evolution of early crack propagation in pitch bearings.

All the work mentioned above considered the pitch bearing as a low-rotating component. However, unlike continuously rotating bearings, such as wind turbine main bearings, gearbox bearings, and generator bearings, the pitch bearing operates within a very limited rotation angle, typically within 90°. As a result, this non-integer cycle rotation presents a significant challenge when applying conventional vibration analysis methods for the purpose of monitoring blade pitch bearings. Interference from blade flapping and dynamic wind loads can further complicate the condition monitoring signals collected from pitch bearings. This makes the currently available methods difficult to implement pitch bearing monitoring in practice. The purpose of this paper is to tackle this challenge by leveraging the advantages of thermal imaging analysis and deep learning.

2. Setup of experimental test rig

To facilitate the study, a blade pitch bearing test rig was developed in the laboratory, as shown in Figure 1. For simplicity, the test rig is featured by a single row contact ball bearing. The detailed specifications of the bearing can be found in Table 1. In addition, the long-term wind power practice has shown that the outer race is one of the most vulnerable components in the blade pitch bearings. For this reason, 16 strain gauges were evenly attached to the outer race of the bearing using specialized adhesive H610 to precisely detect and analyze the strain distribution of the bearing's outer race. It is presumed that outer race faults will induce a significant change in the local strain on the outer race of the bearing. Therefore, in this study, the results measured by these strain gauges will be employed to verify the thermal imaging analysis results. The specifications of the strain gauges are given in Table 2. In practical scenarios, the external load on the blade bearings arises from both the gravitational pull on the wind turbine blades and the force exerted by the wind. However, replicating such overturning moments in the laboratory to induce bearing deformation is challenging. Consequently, in the experiments of this study, a jack was employed to apply load directly to the shaft, effectively simulating the loads imposed by the wind turbine blades and wind. Although such a load application method may not precisely replicate the time-varying loads experienced by the blade bearing, it effectively induces the necessary deformation required for the study.

a) b) c)

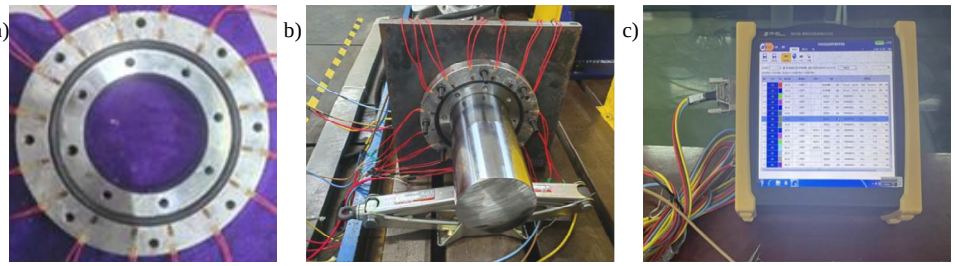

Fig. 1. (a) Bearing used in the test rig; (b) Test rig; (c) Data acquisition system.

Table 1. Specifications of the bearing used in the test rig.

Structural parameter	Numerical value
Outside diameter D/mm	200
Inside diameter D/mm	100
Pitch diameter d m/mm	150
Ball diameter D n/ mm	10
Bearing height H /mm	30
Coefficient of curvature radius of inner ring groove fi	0.525
Coefficient of curvature radius of outer ring groove fe	0.525
Contact Angle α/°	45

Table 2. Specifications of the strain gauges.

Strain gauge parameter	Numerical value
Resistance value /Ω	120±1
Base length * base width /mm	9*4
Grid length * grid width /mm	5*3
Supply voltage /v	3-5
Strain limit /um/m	20000

3. Fault simulation and data acquisition

Given that cracks are a prevalent fault observed on the outer race of the pitch bearing, as depicted in Figure 2a, a simulated crack fault was intentionally introduced onto the outer race of the bearing being tested, as illustrated in Figure 2b.

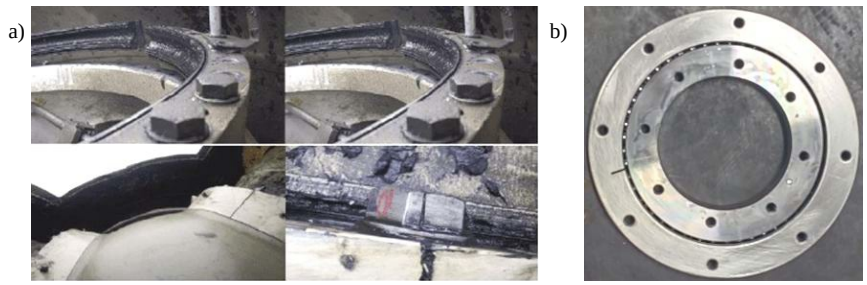

Fig. 2. (a) Real crack fault of blade bearing; (b) Simulated crack on the outer race of the bearing being tested.

In this study, a FLUKE Ti450 infrared camera was employed to capture thermal images of the blade bearing under various health conditions. It is shown in Figure 3, and its detailed specifications are listed in Table 3.

Fig. 3. Thermal camera used in the study.

Table 3. Specifications of the thermal imaging camera FLUKE Ti450.

Main features:	
IFOV (spatial resolution) with standard lens	1.31mRad,D:S 753:1
Detector resolution	320 × 240
Multi-Sharp™ Multi-point focus	Yes, close-up and telephoto images can be captured throughout the view
Laser rangefinder	Yes, calculate the distance to the target to get a precisely focused image.
Temperature measurement:	
Temperature measuring range	−20 ◦C to +1200 ◦C(−4 ◦ F to +2192 ◦ F)
Precision	± 2◦C or 2% (larger value for nominal temperature of 25◦C)
Thermal sensitivity (NETD) filter mode	≤0.05◦C (50mK), target temperature 30◦C
	≤0.03◦C (30mK), target temperature 30◦C

Subsequently, warm up the cracked bearing and collect 1200 thermal images of the bearing when it is at various temperatures. A subset of the thermal images acquired during the experiment is presented in Figure 4.

From Figure 4, it is found that

- regardless of the bearing temperature, the crack on the bearing outer race can be clearly observed from the thermal images collected using the FLUKE Ti450 infrared thermal imaging camera;
- moreover, the higher the bearing temperature, the crack appears to be clearer in the thermal images.

The aforementioned observations indicate the efficacy of employing thermal detection for identifying faults in the outer race of wind turbine blade bearings. One notable advantage of such a condition monitoring approach is the elimination of the need for a sensor directly attached to the blade bearing. Instead, infrared thermal images can be taken from a distance. This addresses the significant challenge of sensor installation in confined spaces, as well as mitigates issues encountered during data collection and transmission.

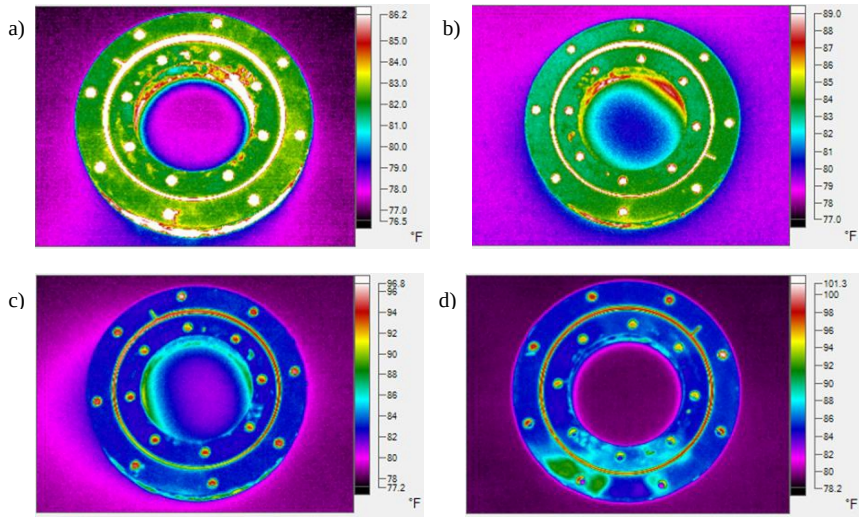

Fig. 4. (a) Image taken at temperature 1; (b) Image taken at temperature 2;
(c) Image taken at temperature 3; (d) Image taken at temperature 4.

4. Artificial fault detection using YOLOv5 model

4.1. Brief introduction of YOLO series of models

The YOLO (You Only Look Once) series comprises end-to-end object detection algorithms, distinguished by their remarkable efficiency in achieving swift detection while maintaining high accuracy. Unlike traditional two-stage detection methods, YOLO directly transforms the object detection task into a regression problem. This unique approach predicts both the object class and bounding box coordinates in a single neural network, eliminating the need for data transfer between multiple modules and significantly enhancing real-time detection speed. One key advantage of the YOLO algorithm is its efficient handling of small objects without the need for intricate preprocessing of training data. This is attributed to its specialized loss function, contributing to its widespread application in practical scenarios.

The YOLO series of algorithms showcases continuous innovation. YOLOv2 and YOLOv3, as representatives, are both end-to-end object detection methods designed for real-time applications. YOLOv2 builds upon its predecessor and addresses various issues through introducing of Batch Normalization, and the use of Anchor Boxes and multi-scale training. Specifically, YOLOv2 adopts the Darknet-19 network architecture and incorporates Batch Normalization, which enhances training stability and showcase improvements over the original YOLO algorithm. YOLOv3 further optimizes YOLOv2 by adopting the deeper Darknet-53 network structure, enhancing feature extraction and detection accuracy. YOLOv3 introduces three different scales of detection, enabling the detection of objects of various sizes and bolstering the algorithm's applicability and robustness. Moreover, YOLOv3 employs more complex loss functions, including classification loss, bounding box coordinate loss, and confidence loss, further optimizing the model and improving detection accuracy.

Building on YOLOv3, YOLOv4 and YOLOv5 represent advanced iterations, boasting higher detection accuracy and faster speeds. YOLOv4 introduces the CSPDarknet53 network architecture on the network of YOLOv3, which utilizes the Cross-Stage Partial Network structure to enhance feature extraction capability and model robustness. By contrast, YOLOv5 takes a different approach, adopting a lightweight network architecture such as CSPNet and leveraging techniques such as reinforcement learning and adaptive training for accelerated model training and exceptional performance in both accuracy and speed. Additionally, YOLOv5 introduces the Adaptive Radius Estimation method, dynamically adjusting the size of object detection bounding boxes, further enhancing the algorithm's robustness and applicability. Both YOLOv4 and YOLOv5 utilize the Spatial Pyramid Pool (SPP) Block structure, a spatial pyramid pooling module capable of handling objects of varying sizes, thereby augmenting the algorithm's applicability and robustness. The diagram of the SPP Block structure is shown in Figure 5.

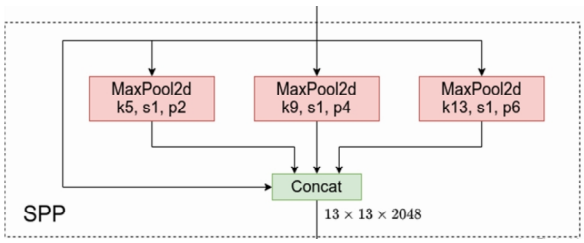

Fig. 5. Diagram of Spatial Pyramid Pool (SPP) Block structure.

Simply speaking, the structure of the YOLO series models consists of four key modules: Input, BackBone, Neck, and Output. Figure 6 illustrates the specific network structure of YOLOv5. From the figure, it becomes evident that the YOLOv5 network structure primarily comprises CBL modules that consist of Convolutional (Conv) layers, Batch Normalization (BN) layers, and Leaky_ReLU activation functions; Resunit residual network modules; BottleneckCSP modules composed of Convolutional layers and multiple Resunit modules; and SPP modules that perform multi-scale fusion using max pooling. These modules are integrated together through tensor concatenation operations for dimension expansion and tensor addition operations for dimension consistency (Yao et al., 2021).

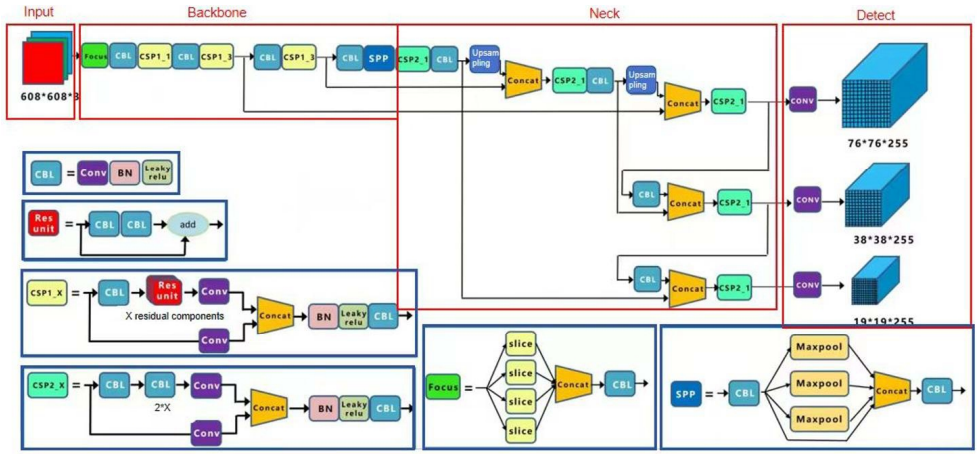

Fig. 6. Network structure of YOLOv5 model.

In the 'Input', YOLOv5 employs the same mosaic data enhancement technique as YOLOv4, exhibiting superior performance in detecting small targets. The Mosaic data augmentation method employs random scaling, cropping, and arrangement on the dataset, yielding two primary advantages. Firstly, the Mosaic technique enhances the dataset's complexity. By applying random scaling and cropping to multiple images and arranging them in a randomized manner, the dataset's diversity is significantly amplified. Notably, the random scaling operation boosts the occurrence frequency of small targets, thereby enhancing the training model's robustness. Introducing more samples with diverse scales, poses, and occlusion variations enables the model to better adapt to a range of real-world scenarios. Secondly, the Mosaic method mitigates GPU memory usage. As the generation of concatenated images involves random scaling and cropping operations, the number of images required to be read for each mini-batch can be minimized. Consequently, even when training with a single GPU, commendable training results can be attained. This reduces hardware resource demands during the training process, thereby enhancing training efficiency and scalability. In addition, YOLOv5 introduces the adaptive anchor frame calculation feature, dynamically computing the optimal anchor frame value during each training session across various datasets.

In 'Backbone', YOLOv5 incorporates the Focus structure to enable efficient slicing operations. For instance, when an original 640×640×3 image is fed into the Focus structure, a slicing operation is applied to generate a 320×320×12 feature map. Following this, a convolution operation with 32 convolution kernels is executed, ultimately constructing a 320×320×32 feature map.

Moving to the 'Neck' component, YOLOv5 utilizes a combination of the Feature Pyramid Network (FPN) - Path Aggregation Network (PAN) structure, the CSP2 structure from Cross Stage Partial Network (CSPNet), and PANet to aggregate features. The neck's primary purpose is to generate feature pyramids, enhancing the model's ability to detect objects of varying scales. This facilitates the recognition of the same object at different sizes and scales. The feature extractor of the network adopts a novel FPN structure, enhancing the bottom-up path and improving the propagation of low-level features.

In 'Detect', the GIOU_Loss loss function and Non-Maximum Suppression (NMS) algorithm are employed to enhance the accuracy and robustness of prediction results. Throughout the training process, the loss function's value signifies the disparity between the model's predictions and the ground truth values. By minimizing this loss function, the model gradually converges, thereby reducing prediction errors and refining the overall fitting of the model. GIOU_Loss function represents an advanced loss function that introduces a correction factor derived from GIOU_Loss function to more precisely evaluate the similarity between predicted boxes and ground truth boxes. Through the optimization of GIOU_Loss function, the model achieves enhanced accuracy in locating target objects and predicting their sizes, thereby elevating the quality of detection results. Finally, the NMS is a technique employed to eliminate overlapping detection boxes. It prioritizes the box with the highest confidence as the primary detection result and suppresses other boxes with significant overlap. This process effectively eliminates redundant detection results, resulting in more precise object detection outputs.

4.2. Training of YOLOv5 model

The hardware used for training the YOLOv5 algorithm includes an Intel(R) Xeon(R) Gold 6226R CPU, a GeForce RTX 3060 GPU, and 128GB of memory. The training process took place on a Windows 10 operating system with CUDA version 11.1. Python 3.8 served as the programming language, and PyTorch was chosen as the deep learning framework.

Then, the thermal images collected from the blade bearing in Section 3 were used to train the YOLOv5 algorithm with the specified parameter configurations: SGD optimization algorithm, a batch size of 2, a maximum of 300 epochs, and a cosine annealing strategy for dynamically adjusting the learning rate, initiated at 0.01. The weight decay coefficient is set to 0.0005, and the momentum factor is 0.937. The GIOU_Loss function serves as the designated loss function. The input image size is 2048×2048, and four images are concurrently trained in each iteration.

As mentioned earlier, image data augmentation technique is commonly used to improve the model's generalization capability. In this study, the following image data augmentation methods were adopted for training YOLOv5 object detection algorithm:

- Random cropping: Randomly selecting a region in the image and cropping it to a fixed size. This simulates different positions and scales of targets in the image;
- Random scaling: Randomly changing the size of the image, which can vary the scale of targets in the image, enhancing the model's ability to recognize objects of different scales;
- Random flipping: Randomly horizontally or vertically flipping the image, enhancing the model's ability to recognize targets from different perspectives;
- Random rotation: Randomly rotating the angle of the image, simulating changes in the appearance of targets at different angles;
- Random adjustments to brightness, contrast, and saturation: Randomly adjusting the image's brightness, contrast, and saturation, improving the model's ability to recognize targets under different lighting conditions.

For YOLOv5 algorithm in this paper, training involves simultaneously processing four images. Some random operation results obtained during training process are illustrated in Figure 7.

During the training process, several important metrics are used to evaluate the performance of the model. Among them, the 'Box' metric represents the error between the predicted box and the ground truth box using the Generalized Intersection over Union (GIoU) (Rezatofighi, 2019). The GIoU is utilized to measure the accuracy of regression boxes, with values close to 0 indicating higher precision in predicting regression boxes. The 'Objectness' metric assesses the accuracy of object detection, and a value close to 0 signifies higher accuracy in object detection. Additionally, there are two other metrics, Precision and Recall. Precision denotes the ratio of correctly detected objects to the total detected objects, with a value closer to 1 indicating more accurate detection results. Recall represents the ratio of correctly detected objects to the total annotated objects, and a value closer to 1 signifies a higher recall rate, indicating more accurate detection of objects. mAP@0.5 is a commonly used evaluation metric, representing the Average Precision calculated at various Intersection over Union (IoU) thresholds. It is computed by calculating the area under the Precision-Recall curve. A higher mAP value, approaching 1, indicates higher accuracy in object detection by the algorithm. The results of these metrics are shown in Figure 8.

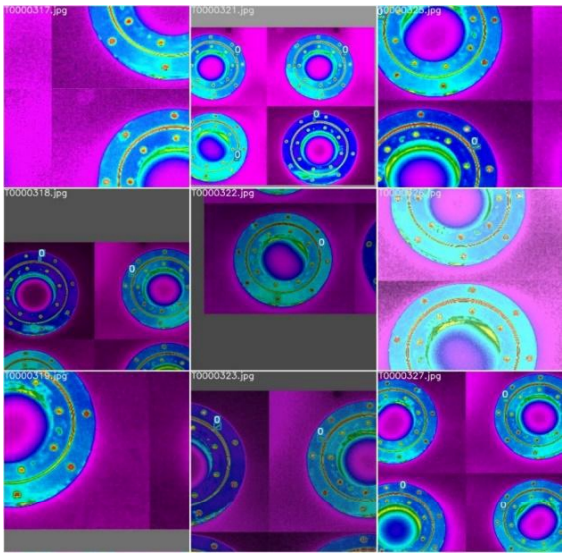

Fig. 7. Part of data augmentation results.

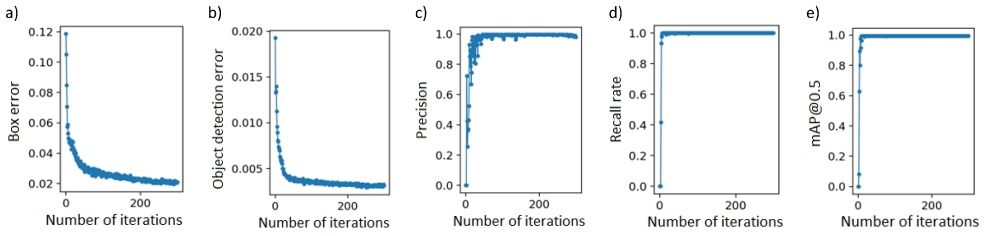

Fig. 8. (a) Box error; (b) Object detection error; (c) Precision; (d) Recall rate; (e) mAP@0.5.

From Figure 8, it can be seen that the YOLOv5 network exhibits a higher detection accuracy for small-scale objects. After computing the training results, the model achieves an average precision (mAP) of 99.5%.

4.3. Verification of the trained YOLOv5 model

To verify the trained YOLOv5 model, 500 infrared thermal images taken from both normal and cracked bearings were randomly selected from the image database. Then, the trained YOLOv5 model was applied to analyze the images. A subset of the crack detection results is illustrated in Figure 9. Obviously, the trained YOLOv5 model correctly discriminated normal and correct bearings, accurately identifying the presence of cracks on the outer race of the blade bearing and achieving a 100% accuracy rate.

5. Conclusions

To tackle the challenge of monitoring the health condition of wind turbine blade bearings operating in non-integer cycles, this paper introduces an intelligent technology for blade bearing condition monitoring, leveraging infrared thermal detection and the YOLOv5 artificial neural network model. The experimental results have demonstrated that:

- Infrared thermal detection emerges as a highly effective method for detecting crack faults in the outer race of blade pitch bearings. Its notable advantage lies in its capacity to capture images from a considerable distance. This surpasses traditional non-destructive testing methods, obviating the need for sensor installation. It also exhibits significant advantages in data collection and transmission.

- The YOLOv5 model exhibits outstanding superiority and robust detection capabilities, particularly in the realm of small object detection. In this study, the trained YOLOv5 model demonstrated an impressive average detection accuracy of 99.5%.

Encouraged by the achievements in this paper, the future research endeavors will delve into further exploring the capabilities of the proposed technology for detecting various types of faults in blade pitch bearings beyond the scope of this study that only considered the detection of cracked outer race fault.

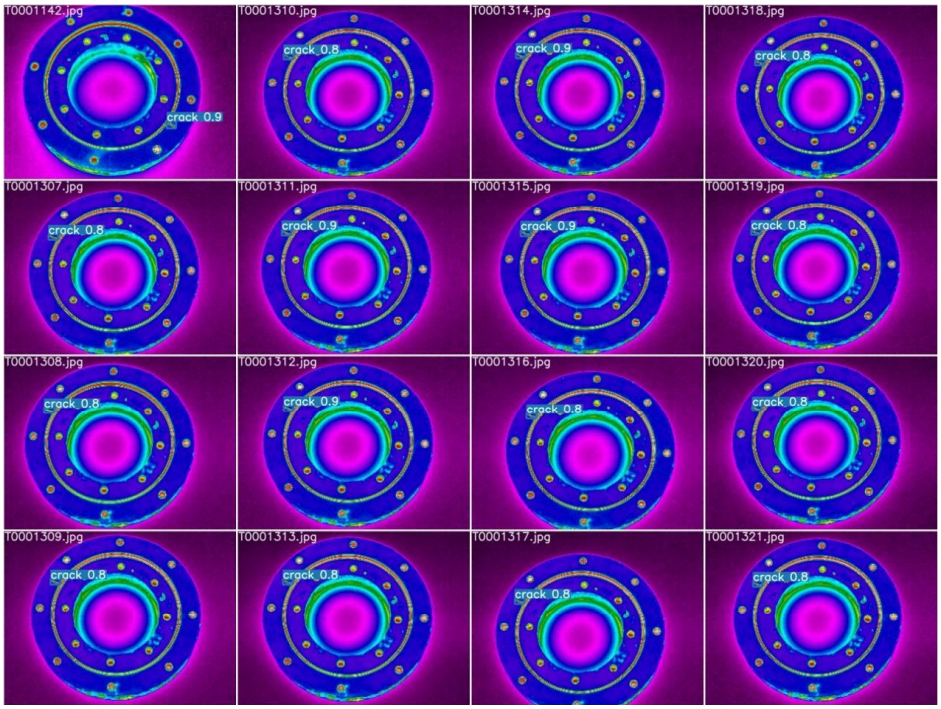

Fig. 9. Part of the object detection results generated by YOLOv5 model.

Acknowledgements

The work reported above was supported by the National Natural Science Foundation of China (52175089, 12002125), the Natural Science Foundation of Hunan Province (2020JJ6020), and Hunan Provincial Postgraduate Research Innovation Project (CX20211267).

References

Bai, X., Xiao, H., Zhang, L. 2011. The condition monitoring of large slewing bearing based on oil analysis method. Key Engineering Materials, 474-476.

Bi, R., Qian, K., Zhou, C., Hepburna, D.M., Rong, J. 2014. A survey of failures in wind turbine generator systems with focus on a wind farm In: China. International Journal of Smart Grid and Clean Energy 3(4), 366-373.

Chen, Y., Jin, X., Yue, Y., Wang, S., Han, H., Wen, M., Wang, Q., Cheng, P., 2023. Investigation on 3D fatigue crack propagation in pitch bearing raceway of offshore wind turbines. Ocean Engineering 269, 113524.

GWEC. 2023. Global Wind Report 2023. https://gwec.net/globalwindreport2023.

He, L., Hao, L., Pan, D., Qiao, W., 2019. Detection of single-axis pitch bearing defect in a wind turbine using electrical signature analysis. Proceedings of 2019 IEEE International Electric Machines & Drives Conference (IEMDC). DOI: 10.1109/IEMDC38053.2019.

Hofmann, M., Sperstad, I.B. 2014. Will 10 MW wind turbines bring down the operation and maintenance cost of offshore wind farms?. Energy Procedia 53, 231-238.

Kandukuri, S.T., Senanyaka, J.S.L., Huynh, V.K., Robbersmyr, K.G. 2019. A two-stage fault detection and classification scheme for electrical pitch drives in offshore wind farms using support vector machine. IEEE Transactions on Industry Applications 55(5), 5109-5118.

Liu, R. 2007. Condition monitoring of low-speed and heavily loaded rolling element bearing. Industrial Lubrication and Tribology 59(6), 297–300.
Liu, Z., Wang, X., Zhang, L. 2020. Fault diagnosis of industrial wind turbine blade bearing using acoustic emission analysis. IEEE Transactions on Instrumentation and Measurement 69(9), 6630-6639.
Liu, Z., Zhang, L. 2019. Naturally damaged wind turbine blade bearing fault detection using novel iterative nonlinear filter and morphological analysis. IEEE Transactions on Industrial Electronics 67(10), 8713-8722.
Liu, Z., Zhang, L., Carrasco, J., 2020, Vibration analysis for large-scale wind turbine blade bearing fault detection with an empirical wavelet thresholding method. Renewable Energy 146, 99-110.
National Development and Reform Commission. 2015. Study on scenario and path of China's high proportion of renewable energy development in 2050. https://www.efchina.org/Attachments/Report/report-20150420/China-2050-High-Renewable-Energy-Penetration-Scenario-and-Roadmap-Study-Executive-Summary.pdf.
Pan, D., Hao, L., He, L., Grubic, S. 2019. System and method for detecting pitch bearing damage in a wind turbine, US Patent US10273940B2.
Pan, Y., Hong, R., Chen, J., Qin, Z., Feng, Y. 2019. Incipient fault detection of wind turbine large-size slewing bearing based on circular domain. Measurement 137, 130-142.
Plaza, J., Abasolo, M., Coria, I., Aguirrebeitia, J., Bustos, I. F. 2015. A new finite element approach for the analysis of slewing bearings in wind turbine generators using superelement techniques. Meccanica 50, 1623-1633.
Rezatofighi, H., Tsoi, N., Gwak, J., Sadeghian, A., Reid, I., Savarese, S. 2019. Generalized intersection over union: A metric and a loss for bounding box regression. Proceedings of the IEEE/CVF Conference on Computer Vision and Pattern Recognition, 658-666.
Sandoval, D., Leturiondo, U., Pozo, F., Vidal, Y. 2020. Low-speed bearing fault diagnosis based on permutation and spectral entropy measures. Applied Sciences 10(13), 4666.
Van Hecke, B., Yoon, J., He, D. 2016. Low speed bearing fault diagnosis using acoustic emission sensors. Applied Acoustics 105, 35-44.
Vásquez, S., Kinnaert, M., Pintelon, R. 2019. Active fault diagnosis on a hydraulic pitch system based on frequency-domain identification. IEEE Transactions on Control Systems Technology 27(2), 663-678.
Wei, L., Qian, Z., Zareipour, H. 2020. Wind turbine pitch system condition monitoring and fault detection based on optimized relevance vector machine regression. IEEE Transactions on Sustainable Energy 11(4), 2326 – 2336.
Wilkinson, M., Hendriks, B., Spinato, F. et al. 2010. Methodology and results of the reliawind reliability field study. In: European Wind Energy Conference (EWEC 2010), 20-23 Apr 2010, Warsaw, Poland.
Yao, J., Qi, J, Zhang, J., Shao, H., Yang, J., Li, X. 2021. A real-time detection algorithm for Kiwifruit defects based on YOLOv5. Electronics 10(14), 1711.
Zhang, C., Liu, Z., Zhang, L. 2022. Wind turbine blade bearing fault detection with Bayesian and Adaptive Kalman Augmented Lagrangian algorithm. Renewable Energy 199, 1016-1023.
Zhang, C., Márquez, F.P.G., Zhang, L. 2022. Artificial intelligence techniques and cloud computing for wind turbine pitch bearing fault detection. Non-Destructive Testing and Condition Monitoring Techniques In Wind Energy, Elsevier BV.
Zvokelj, M., Zupan, S., Prebil, I. 2010. Multivariate and multiscale monitoring of large-size low-speed bearings using Ensemble Empirical Mode Decomposition method combined with principal component analysis. Mechanical Systems and Signal Processing 24(4), 1049-1067.